

# An unconventional adaptation of a classical Gaussian plume dispersion scheme for the fast assessment of external irradiation from a radioactive cloud

Petr Pecha<sup>1</sup>, Emilie Pechova<sup>2</sup>

<sup>1</sup> Institute of Information Theory and Automation of the Czech Academy of Sciences, v.v.i.,  
Pod Vodarenskou vezi 4, 182 08, Prague 8, Czech Republic

<sup>2</sup> Institute of Nuclear Research, Div. EGP, 250 68 Rez near Prague, Czech Republic

E-mail: [pecha@utia.cas.cz](mailto:pecha@utia.cas.cz)

## Abstract

This article focuses on derivation of an effective algorithm for the fast estimation of cloudshine doses/dose rates induced by a large mixture of radionuclides discharged into the atmosphere. A certain special modification of the classical Gaussian plume approach is proposed for approximation of the near-field dispersion problem. Specifically, the accidental radioactivity release is subdivided into consecutive one-hour Gaussian segments, each driven by a short-term meteorological forecast for the respective hours. Determination of the physical quantity of photon fluence rate from an ambient cloud irradiation is coupled to a special decomposition of the Gaussian plume shape into the equivalent virtual elliptic disks. It facilitates solution of the formerly used time-consuming 3-D integration and provides advantages with regard to acceleration of the computational process on a local scale. An optimal choice of integration limit is adopted on the basis of the mean free path of  $\gamma$ -photons in the air. An efficient approach is introduced for treatment of a wide range of energetic spectrum of the emitted photons when the usual multi-nuclide approach is replaced by a new multi-group scheme. The algorithm is capable of generating the radiological responses in a large net of spatial nodes. It predetermines the proposed procedure such as a proper tool for online data assimilation analysis in the near-field areas. A specific technique for numerical integration is verified on the basis of comparison with a partial analytical solution. Convergence of the finite cloud approximation to the tabulated semi-infinite cloud values for dose conversion factors was validated.

**Keywords:** Photon fluence, atmospheric dispersion, cloudshine dose

## 1. Introduction

The main goal of this article is to formulate a fast and sufficiently accurate approach for estimation of the cloudshine irradiation doses which replaces the former rough estimations. The shape of a radioactive plume in the atmosphere near the source of pollution is narrow (especially for a stable atmospheric stratification like category *F*) and does not noticeably diffuse to the surface until it has travelled a distance of several kilometres from the point of discharge (even more than 10 km for a buoyant plume). Due to the buoyant and vertical momentum plume rise the effective height can markedly increase. The vertical concentration profile is gradually getting homogenous only from greater distances. Common practice introduces the calculation of the ground-level cloudshine dose rates at larger distances as a product of this homogenised near-ground activity concentration and the tabulated conversion coefficient  $R_{cloud}$  ( $Sv.m^3.Bq^{-1}.s^{-1}$ ) defined in (ICRP 74, 1996). The technique of the irradiation calculations is designated as a semi-infinite cloud approach. Its application at near distances can, however, cause huge errors and the real finite plume shape should be respected. Further development led to the time-consuming calculations based on a three-dimensional integration over the finite cloud volume (e.g. ADMS4, 2009, Overcamp, 2007) or on a specially partitioned integration space (Wang *et al.*, 2004, Raza *et al.*, 2001). The 3-D integration of the Gaussian plume is fairly complex and computationally expensive, and in many cases sufficiently accurate approximations

53 could be constructed. The volume integral for gamma doses was formerly approximated by using the  
54 semi-infinite cloud model combined with correction factors. The first attempt to solve the problem  
55 was the former approach based on introduction of a certain tabulated finite cloud correction factors  
56  $F^{cor}$  (Slade, 1968). The similar approach based on a pre-calculated matrix of the cloud gamma  
57 correction factors was used in (ATSTEP, 2000) - parameterisation in the photon energy, horizontal  
58 dispersion coefficient, roughness length, plume height, and stability class. An analogical procedure is  
59 used in (Thykier-Nielsen et al., 1995) in the Lagrangian puff model RIMPUFF for the calculation of  
60 gamma doses from assymetrical puffs. The multi-parameter gamma dose values are pre-calculated as a  
61 function of the photon energy, horizontal dispersion and asymmetry factor, height of puff centre and  
62 the distance from the puff base point. We have two main objections to the pre-calculated procedures.  
63 Firstly, due to the steep gradients of activity concentration a suitable interpolation on the fixed spatial  
64 grid could be problematic. Secondly, we have to include possible elevated locations of the receptors  
65 (e.g. real orography of the terrain, monitoring towers). Our proposed method inherently solves the 3-D  
66 configuration of the receptors, which can be crucial for the determination of a dangerous flight levels  
67 for an aircrew during the aerial monitoring.

68 An ultimate aim of our research is improvement of the model predictions of this radiological situation  
69 based on assimilation with real observations incoming from the terrain. The assimilation procedures  
70 perform statistical merging of the model predictions and the measured values in the observation space.  
71 Its dimension equals the number of monitoring sensors on the terrain and, therefore, a parallel  
72 simulation of the dose rate responses on a large net of receptors in the terrain from a wide group of  
73 leaking radionuclides is essential. At the same time some special online examinations like predicting  
74 the time to the first alarm or investigating the weakest plume detectability can be accomplished. From  
75 a general point of view the fast and effective method for estimation of the finite cloud problem at near  
76 distances facilitates the realisation of the assimilation techniques. Advanced assimilation techniques  
77 coming from sequential Monte-Carlo methods are computationally expensive (e.g. Doucet *et al.*,  
78 2001) and an effective procedure for fast simulation of external irradiation has a crucial significance  
79 (ASIM, 2012). Our first attempts at Bayesian tracking began in (Pecha *et al.* 2009). The recent  
80 application of inverse modelling techniques for extracting of the model parameter information from  
81 the incoming terrain observations is described in (Smidl *et al.* 2013).

## 82 83 84 **2. Predictions of harmful admixture propagation nearby a source** 85

86 This article deals with adaptation of the classical solution of a diffusion equation in the initial phase of  
87 radioactive plume drifting. The analysis should satisfactorily cover the area of a teledosimetric ring of  
88 sensors (TDS) located within a few hundred metres around a source. The 3-D distribution of the  
89 specific radioactivity concentration  $C^n$  of nuclide  $n$  in the air ( $Bq.m^{-3}$ ) is expressed by the straight-line  
90 Gaussian solution. This near-field model has a long tradition of use for dispersion predictions. Even  
91 though it is simple, the Gaussian model is consistent with the random nature of turbulence (Hanna *et al.*,  
92 1982). It is a solution of the Fickian diffusion equation for constant diffusivity coefficient  $K$  and  
93 average plume velocity  $\bar{u}$ . The model is tuned to experimental data and offers quicker estimation with  
94 a reasonable computational effort. Proved semi-empirical formulae are available for approximation of  
95 important effects such as interaction of the plume with *near-standing buildings* or momentum and  
96 buoyant *plume rise* during release. Semi-empirical formulae are introduced for estimation of the wind  
97 speed *changes with height* and for *depletion* of the plume radioactivity due to the *removal processes* of  
98 dry and wet deposition and radioactive decay. Separate transport mechanisms of radioactivity  
99 according to the *physical-chemical forms* of admixtures and *landuse characteristics* are considered.  
100 The effects of small changes of *surface elevation* and *terrain roughness* on atmospheric dispersion can  
101 be approximately included.  
102

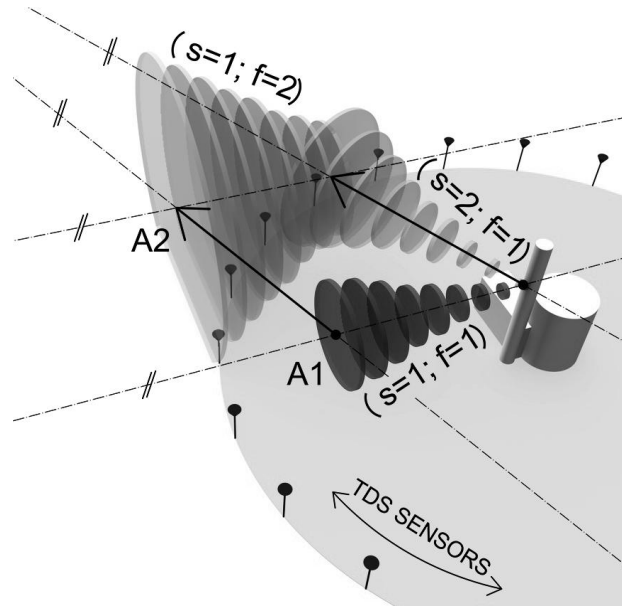


**Figure 1.** The finite cloud propagation during stepwise changes of meteorological conditions. Weather changes observed/forecast for the point of release for a particular time step  $\Delta T^{segm}$  are assumed to immediately impact the propagation of all previous segments in their corresponding phases.

Let assume the continuous radioactivity release to be decomposed into consecutive time segments  $s$ . The straight-line Gaussian solution is taken for description of each segment  $s$  in its first time step  $\Delta T^{segm}$  of propagation within the time interval  $\langle 0; \Delta T^{segm} \rangle$ . In the subsequent time phases  $f$  of the segment  $s$  the meteorological conditions have to be considered more realistically. For this purposes a segmented Gaussian plume model (SGPM) is introduced (Hofman and Pecha, 2011). The model together with the algorithm proposed here is fully integrated into the environmental code HARP (HAZARDOUS Radioactivity Propagation). The model SGPM is initiated from the first phase  $f=1$  of the straight-line propagation supposing the longitudinal dispersion is neglected. The analytical shape of the partial plume confined on interval  $x \in \langle 0; \Delta T^{segm} \cdot \bar{u} \rangle$  is described by expression (1). In the consecutive phases  $f > 1$  the segment  $s$  is drifted according to the current changes of meteorological conditions. The further dispersion and deposition (e.g.  $(s=1; f=1) \rightarrow (s=1; f=2)$  in Figure 1) is simulated using the SGPM algorithm by means of a large number of elemental shifts driven by the new weather conditions (HARP, 2011). During each shift the activity depletion in the cloud due to dry and wet deposition and radioactivity decay is assumed. A complicated scenario of a release time progress is synchronized with the available meteorological observations/forecasts.

The plume is assumed to be driven through the near vicinity by weather forecast given for the point of release. The time step of extents  $\Delta T^{segm}$  should be selected according to accessibility of the meteorological data (one-hour or half an hour). During each time interval  $\Delta T^{segm}$  a new set of the local observed/forecast meteorological data is assumed to be available in the nearest vicinity of the source. We can hardly expect to have the weather data in a fine spatial and time resolution (let us say for a few hundred meters from the source). We have adopted a certain intuitive subjective assumption for the plume spread in the nearest vicinity according to the sketch shown in Figure 1. In this case the weather changes observed/forecast for the point of release for a particular time step  $\Delta T^{segm}$  immediately and in the same way impact the propagation of all segments in their corresponding phases. The interval  $\Delta T^{segm}$  of on-site meteorological measurements is typically from several minutes to one hour. Besides information related to the source of release we are also using a short-term meteorological forecast: 48 hours forward on the spatial grid on an area of  $200 \times 200$  km around the source of pollution. It enables us to connect the plume tracing at larger distances with the previous nearest-range analysis.

The initial straight-line plume propagation during the time step extent  $\Delta T^{segm}$  is simulated by simplified solution of the diffusion equation in the form:

$$\begin{aligned}
139 \quad C^n(x, y, z) &= \frac{A^n}{2\pi \cdot \sigma_y(x) \cdot \sigma_z(x) \cdot \bar{u}} \cdot \exp\left(-\frac{y^2}{2\sigma_y^2(x)}\right) \cdot \left[ \exp\left(-\frac{(z-h_{ef})^2}{2\sigma_z^2(x)}\right) + \exp\left(-\frac{(z+h_{ef})^2}{2\sigma_z^2(x)}\right) + \right. \\
140 \quad &\left. + \exp\left(-\frac{(z-2H_{mix}+h_{ef})^2}{2\sigma_z^2(x)}\right) + \eta_{JV}(x, z) \right] \cdot f_R^n(x) \cdot f_F^n(x) \cdot f_W^n(x)
\end{aligned} \tag{1}$$

- 141  $C^n(x, y, z)$  Specific activity of radionuclide  $n$  in spatial point  $(x, y, z)$  in  $(Bq \cdot m^{-3})$ ;  
142  $x$  – direction of spreading;  $y, z$  – horizontal and vertical coordinates  
143  $\sigma_y(x), \sigma_z(x)$  Horizontal and vertical dispersion coefficients at distance  $x$  from the source ( $m$ );  
144 expressed by empirical formulae  
145  $A^n$  Continuous release source strength of nuclide  $n$  ( $Bq \cdot s^{-1}$ ); continuous and constant  
146 within the time interval  $\Delta T^{segm}$   
147  $\bar{u}$  Mean advection velocity of the plume in direction  $x$  ( $m \cdot s^{-1}$ )  
148  $h_{ef}, H_{mix}$  Effective height of the plume axis over the terrain ( $m$ ), height of planetary mixing  
149 layer ( $m$ )  
150  $\eta_{JV}(x, z)$  Effect of additional multiple reflections on ground and inversion layer/mixing height  
151 (for this near-field model hereafter ignored)  
152  $f_R^n, f_F^n, f_W^n$  Plume depletion factors due to radioactive decay and dry and wet deposition. The  
153 latter two are dependent on the physical-chemical form (aerosol, organic, elemental)  
154 of nuclide  $n$ . The factors stand for the “source depletion” approach introduced into the  
155 classical straight-line Gaussian solution. The release source strength at distance  $x$  is  
156 depleted according to  $A^n(x, y=0, z=h_{ef}) = A^n(x=0, y=0, z=h_{ef}) \cdot f_R^n(x) \cdot f_F^n(x) \cdot f_W^n(x)$   
157 -- more in (HARP, 2011).  
158

159 The exponential terms in equation (1) from left to right mean the basic diffusion growth of the  
160 plume, its reflection in the ground plane and its reflection from the top of mixing layer  $H_{mix}$ . The  
161 designed atmospheric dispersion model SGPM was compared with international codes COSYMA and  
162 RODOS (Pecha and Pechova, 2002; HARP, 2011). The documentation of the HARP system and other  
163 additional comparisons are described in detail in (HARP, 2011). The applicability of the straight-line  
164 propagation in the first hour of a release is limited on the near field areas inside the emergency  
165 planning zone around a nuclear facility up to 15 - 20 kilometres. For a simple scenario the results are  
166 well comparable with the time consuming techniques based on Lagrangian particle dispersion models  
167 (e. g. NAME III (Bedwell *et al.*, 2010); Armand *et al.*, 2005)) - see Section 6.  
168

### 169 3. Proposition of the fast scheme for evaluation of external irradiation from radioactive cloud

170  
171 We shall consider the physical quantity of the photon fluence which represents a number of  
172 monoenergetic  $\gamma$  photons with energy  $E_\gamma$  passing through a specific area. Transport of photons with  
173 energy  $E_\gamma$  from the source of emission to the receptors R will be described by the quantity of photon  
174 fluence rate  $\Phi(E_\gamma, R)$  in units  $(m^{-2} \cdot s^{-1})$ . External exposure from the finite plume can be estimated  
175 when applying traditional methods based on three-dimensional integration over the cloud (e.g.  
176 ADMS4, 2009) or on specially constructed three-dimensional columned space divided into many  
177 finite grid cells (e.g. Wang *et al.*, 2004). Photon fluence rate at a receptor point R on the terrain from  
178 the whole plume volume  $V_{plume}$  emitting monoenergetic  $\gamma$ -photons of energy  $E_\gamma$  is calculated  
179 according to the three-dimensional integration given by equation (2).

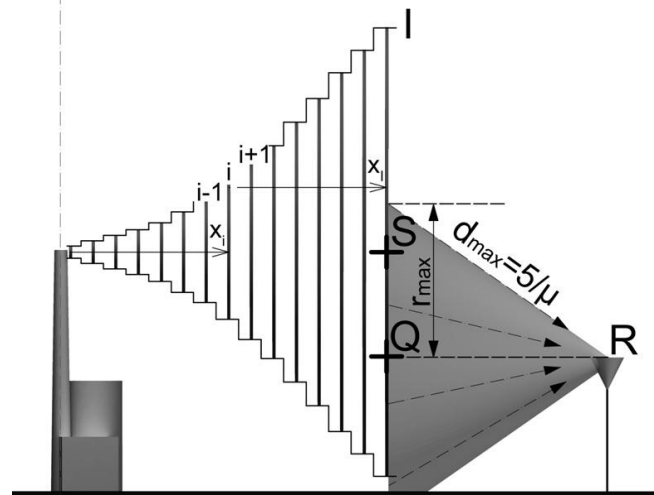
$$180 \quad \Phi_{total}(E_\gamma, R) = \iiint_{V_{plume}} \frac{f^n(E_\gamma) \cdot C^n(x, y, z) \cdot B(E_\gamma, \mu(E_\gamma) \cdot d) \cdot \exp(-\mu(E_\gamma) \cdot d)}{4\pi d^2} dV \tag{2}$$

181 where  $\mu(E_\gamma)$  is the linear attenuation factor ( $m^{-1}$ ),  $d$  denotes the distance between the receptor point R  
182 and the plume elemental volume  $dV$ .  $B(E_\gamma, \mu(E_\gamma) \cdot d)$  stands for the build-up factor. We use its linear  
183 form  $B(E_\gamma, \mu \cdot d) = 1 + k \cdot \mu \cdot d$ . Here  $k = (\mu - \mu_a) / \mu_a$ ,  $\mu_a$  stands for the linear energy absorption coefficient

184 ( $\text{m}^{-1}$ ). Both coefficients are related to the monoenergetic photons with energy  $E_\gamma$ . Comparison of the  
 185 linear form with the alternative Berger's formula can be found in literature, e.g. in (Overcamp, 2007).  
 186 Specifically, we can assume the monoenergetic  $\gamma$ -photons emitted by the radionuclide  $n$ . The value  
 187  $f^n(E_\gamma)$  is the branching ratio for radionuclide  $n$  to the specified energy  $E_\gamma$ . Activity concentration  $C^n$  of  
 188 radionuclide  $n$  in the air is given by the analytic equation (1).

189 Continuous and constant release in direction of axis  $x$  with average velocity  $\bar{u}$  is partitioned into an  
 190 equivalent number of elliptic discs according to Figure 2. The thickness of the discs  $\Delta x$  was tested for  
 191 the optimal choice (see conclusion in Table 1 below). The centre of the disc  $i$  reaches the position  $x_i =$   
 192  $(i-1/2) \times \Delta x$  in  $x_i / \bar{u}$  seconds. A discrete technique is introduced when the model parameters are  
 193 averaged within interval  $\Delta x$  on the disc  $i$ . Distribution of the activity concentration in the disc  $i$  on the  
 194 plane  $x = x_i$  (it means the average value on  $\Delta x$ ) is driven according to the straight-line equation (1)  
 195 where the corresponding averaged disc parameters are inserted (e.g.  $x_i$ ,  $\sigma_y(x_i)$ ,  $\sigma_z(x_i)$ , depletion  
 196 factors  $f_R^n(x_i) \cdot f_F^n(x_i) \cdot f_W^n(x_i)$  etc.).

197 The  $5/\mu(E_\gamma)$  method (Wang *et al.*, 2004) (generally  $m/\mu(E_\gamma)$  method – the values  $m=5,10,15$  were  
 198 tested) imposes an integration limit up to  $d_{max}$  and indicates as significant only those sources of  
 199 irradiation that lie within a distance of  $5/\mu(E_\gamma)$  from the receptor R. The integration boundary (see also  
 200 the integration circle in Figure 3) is formed by intersection of the cone (receptor R is in the cone  
 201 vertex) and the plane of the newest disc  $I$ . Only the points located inside are assumed to contribute to  
 202 the fluence rate at R. This markedly accelerates the computational speed and improves the capability  
 203 of the assimilation procedures to run successfully in real time mode. It can, for a near-field problem,  
 204 serve as an effective alternative to computationally expensive traditional methods based on full 3-D  
 205 integration techniques (Raza *et al.*, 2001).



206

207 **Figure 2.** Partitioning of continuous Gaussian shape into equivalent elliptical disc sequence  $i$  ( $i=1, \dots, I$ ).  
 208 Irradiation of receptor R from the last disc  $I$  is illustrated.  
 209

210 A substantial performance improvement makes the  $5/\mu(E_\gamma)$  approach the first choice for its  
 211 application during nuclear emergency situations (Wang *et al.*, 2004). Minor differences from the  
 212 traditional methods of coarse 3-D integration are referred to here for a broad range of input model  
 213 parameters (stability classes, axial distances, source term characteristics etc.). The partial results of  
 214 spatial progression for stability classes F and D are given in Figure 5 below. A comparison benchmark  
 215 of the results with several European codes is presented in Section 6.2.  
 216

## 217 4. Replacement of traditional 3-D integration by stepwise 2-D computational scheme

### 218 4.1 Formulation of the stepwise 2-D computational approach

219 External irradiation from the plume section on interval  $\langle x_i - \Delta x/2; x_i + \Delta x/2 \rangle$  is substituted by an  
 220 equivalent effect of a disc of thickness  $\Delta x$  with averaged model parameters on  $\langle x_i - \Delta x/2; x_i + \Delta x/2 \rangle$ .  
 221 Let us analyse the contribution to the fluence rate at the receptor R from irradiation with

222 monoenergetic photons having energy  $E_\gamma$  from the elliptical disc  $I$ . A lateral view of the partitioned  
 223 plume propagation is demonstrated in Figure 2. The same situation is outlined in the front view in  
 224 Figure 3. The boundary of the integration region lying in the plane of disc  $I$  is based on  
 225  $5/\mu(E_\gamma)$  approximation (bold dashed line composed of the part of the circle above ground with a radius  
 226 of  $r_{max}$  and with its centre in the point Q). For  $r_{max}$  the relationship  $r_{max}^2 = (5/\mu(E_\gamma))^2 - [x(R) - x(Q)]^2$   
 227 holds true. The points S and Q are lying in the plane of disc  $I$  (S is its centre, the abscissa RQ is  
 228 perpendicular to the plane). Contribution of the disc  $I$  with unit thickness  $\Delta x=1$  m to the photon  
 229 fluence rate at receptor R is given by:  
 230

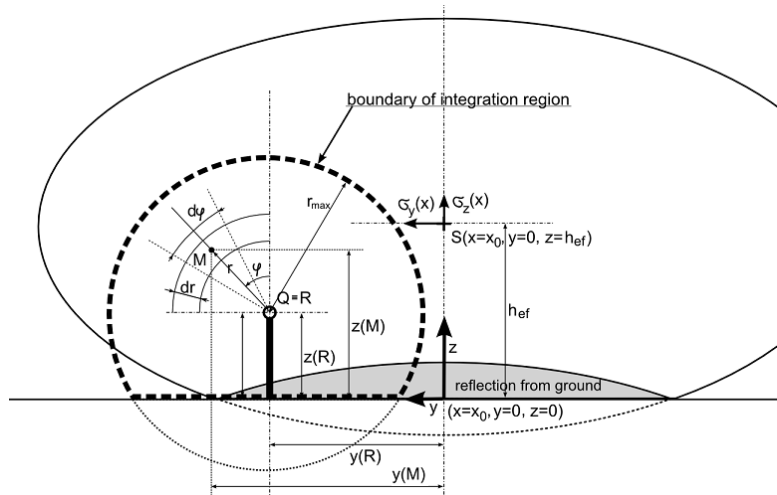
$$231 \quad \Phi^{\Delta x=1}(E_\gamma, R, I, x_I) = \frac{1}{4\pi} \int_{r=0}^{r_{max}} \int_{\varphi=0}^{2\pi} \frac{f^n(E_\gamma) C^I(x_I; r, \varphi) \cdot B(E_\gamma, \mu(E_\gamma) \cdot d) \cdot \exp(-\mu(E_\gamma) \cdot d)}{d^2} r d\varphi dr$$

(3a)

232 The contribution from the disc  $I$ , which in general has a thickness of  $\Delta x$ , can be roughly expressed as:  
 233

$$234 \quad \Phi(E_\gamma, R, I) = \Delta x \cdot \Phi^{\Delta x=1}(E_\gamma, R, I, x_I) \quad (3b)$$

235 Referring to Figure 3, the value of  $d$  is distance between points R ( $x(R), y(R), z(R)$ ) and M ( $x(M), y(M), z(M)$ );  
 236  $d^2 = (x(S) - x(R))^2 + (y(M) - y(R))^2 + (z(M) - z(R))^2$ ;  $x(S) = x_I = (I-1/2) \times \Delta x$  is the distance of  
 237 the centre of the disc  $I$  from the release point;  $y(M) = y(R) + r \times \sin(\varphi)$ ;  $z(M) = z(R) + r \times \cos(\varphi)$ . The  
 238 equivalent specific source strength  $C^I(x_I, y, z)$  of emitted monoenergetic photons in the disc  $I$  is  
 239 expressed using  $C^n$  from equation (1) multiplied by branching ratio  $f^n(E_\gamma)$ . Valid values of coordinate  $z$   
 240 should be positive, dispersion coefficients and depletion factors are calculated for position  $x_I$  (it means  
 241 for a time of  $x_I/\bar{u}$  seconds) and are dependent on the physical-chemical form of the respective  
 242 radionuclide.



243  
 244  
 245 **Figure 3.** (Coupled with Figure 2): Frontal view from the receptor point R to the elliptical disc  $I$  and circular  
 246 integration region (bold dashed line).  
 247

248 An equivalent source strength for the disc  $I$  includes source depletion model and substitutes the  
 249 original discharge from equation (1) according to  $A(x_I, y=0, z=h_{ef}) = A(x=0, y=0, z=h_{ef}) \cdot f_R(x_I) \cdot f_F$   
 250  $(x_I) \cdot f_W(x_I)$ . During computation the values of photon fluence rates are gradually stored into the array  
 251  $F(1:N_{sens}, 1:I_{total})$ . Here  $N_{sens}$  means the number of receptors being simultaneously taken into account,  
 252 and  $I_{total}$  stands for the total number of discs with thickness  $\Delta x$  of the plume separation ( $I_{total}$  is in  
 253 order of  $10^3$ ). The total fluence rates, total fluencies and the corresponding total cloudshine doses/dose  
 254 rates are generated by processing of the array values in the particular time steps  $x_i/\bar{u}$ ,  $i=1, \dots, I_{total}$ .

#### 255 4.2. Selecting the computational grid size in practice

256 The proposed stepwise numerical scheme is shown in Figure 2. The precision of calculations on the  
 257 one hand and computational time on the other hand depend on the choice of the disc thickness  $\Delta x$

258 entering the equation (3). Thickness of the discs was tested for selected values  $\Delta x = 1\text{m}, 10\text{m}, 50\text{m}$   
 259 (see the conclusions in Table 1 below). Table 1 demonstrates the importance of an effective choice of  
 260 the thickness value  $\Delta x$ . Fine resolution  $\Delta x=1\text{m}$  leads to about 50 times prolongation of the calculations  
 261 with respect to the rough grid  $\Delta x=50\text{m}$ . The latter one gives some differences, mainly at locations  
 262 near the source of pollution. Practically all computations were performed with  $\Delta x = 10\text{m}$  proposed  
 263 here as an optimum compromise between the precision and speed of computation. The affirmation  
 264 should be valid for all nuclides ( $^{133}\text{Xe}$  has almost the lowest  $\bar{E}^{^{133}\text{Xe}}$  (see Table 4) and does have the  
 265 lowest mean free path in air).

266

267 **Table 1.** Photon fluence rate induced by a plume as a function of  $\Delta x$  from equation (3b). Responses on sensors  
 268 TST01 and TST02 just  $T_{\text{minute}}$  after the start of continuous release of  $^{133}\text{Xe}$  with source strength from Table 4.

269

Duration of release is 1 hour.

Sensor <sup>b</sup>	$T_{\text{minute}}(\text{min})$	Photon fluence rate ( $\text{m}^{-2}\cdot\text{s}^{-1}$ ) <sup>a</sup>		
		$\Delta x=1\text{m}$	$\Delta x=10\text{m}$	$\Delta x=50\text{m}$
TST01	5	1.568 E+11	1.452 E+11	8.180 E+10
TST01	6	4.745 E+11	4.786 E+11	4.727 E+11
TST01	$\geq 8^c$	5.485 E+11	5.483 E+11	5.373 E+11
TST02	20	1.101 E+11	1.035 E+11	1.259 E+11
TST02	$\geq 23^c$	2.813 E+11	2.760 E+11	2.469 E+11
Relative time of computation up to 1 hour of the cloud propagation		1.0	~0.10	~0.02

270

<sup>a</sup> continuous release of radionuclide  $^{133}\text{Xe}$  with the source strength  $2.28 \text{ E}+14 \text{ Bq}\cdot\text{s}^{-1}$

271

<sup>b</sup> TST01 , TST02 are located at 400 m and 1500 m respectively from the source

272

<sup>c</sup> equilibrium values of photon fluence rate are constant up to the end of the continuous release

273

274 However, the equilibrium values can apparently be generated even with rough grid sizes. The values  
 275 of the photon fluence rates at certain positions can reach their equilibrium values during a long-lasting  
 276 release and remain constant for the remaining progress of the plume (e.g. see constant part of the  
 277 courses in Figure 4 left).

278

279

## 280 5. Formulation of the fast computational procedure in the initial phase of the plume 281 propagation

282

283 The subsequent post-processing of the array  $F$  described above provides a sufficient approximation to  
 284 the basic solution described by equation (3). Figure 2 shows the scheme for the fragmentation of the  
 285 plume shape into the consecutive virtual elliptical discs. The first segment of propagation during the  
 286 time steps  $\Delta T^{\text{egm}}$  is assumed to be described by the corresponding part of straight-line Gaussian  
 287 formula. In the following text we shall examine a basic task, namely a linear drifting of the segment in  
 288 its first phase  $f=I$  (described in Figures 1 and 2) and generation of responses in a large net of sensors.  
 289 The analysis for the first phase  $f=I$  is of essential significance because it comprises the teledosimetric  
 290 ring of sensors (TDS) on the fence of the nuclear power plant (roughly 25 sensors at distances of  
 291 approximately 500 meters from the hypothetical source of pollution). The ring plays the decisive role  
 292 in re-estimation of the source term of release and some other model parameters on the basis of  
 293 assimilation with incoming terrain measurements.

294 The front of the plume is determined by the position of the latest disc  $I$  of the bundle of discs which  
 295 corresponds to the time of spreading  $t_I = I \times \Delta x / \bar{u}$ . Recurrent formulae for processing an array of  
 296 fluencies can be derived when distinguishing between two situations.

297

### 298 5.1. The continuous release with steady state discharge rate of admixtures persists

299

300 Let us assume the front of the plume has reached the position of the disc  $I$ , and propagation to the  $I+1$   
 301 disc is in progress. Contribution of each elemental disc  $i=1, \dots, I$  to the fluence rate  $\Phi(E_\gamma, R, i)$  at  
 302 receptor  $R$  was calculated in the previous steps and stored in the array  $F$ . The new contribution  $\Phi(E_\gamma,$   
 303  $R, I+1)$  of the disc  $I+1$  is calculated using integration (3). The recurrent formula for overall fluence  
 304 rate at receptor  $R$  can be formally rewritten as:

$$\Phi(E_\gamma, R, i=1, \dots, I+1) = \Phi(E_\gamma, R, i=1, \dots, I) + \Phi(E_\gamma, R, I+1) \quad (4)$$

305

$$\text{where } \Phi(E_\gamma, R, i=1, \dots, I) = \sum_{i=1}^{i=I} \Phi(E_\gamma, R, i)$$

306 Then, the only computation effort is to evaluate 2-D integration of the latest disc  $I+1$ . Analogously,  
 307 the recurrent formula for the entire photon fluence at receptor  $R$  from the same beginning of the  
 308 release is given by:

$$\Psi(E_\gamma, R, i=1, \dots, I+1) = \Psi(E_\gamma, R, i=1, \dots, I) + \sum_{i=1}^{i=I+1} \Delta t_i \cdot \Phi(E_\gamma, R, i) \quad (5)$$

309

$$\text{where } \Psi(E_\gamma, R, i=1, \dots, I) = \sum_{i=1}^{i=I} [(I+1-i) \cdot \Delta t_i \cdot \Phi(E_\gamma, R, i)]$$

310  $\Delta t_i = \Delta t = \Delta x / \bar{u}$  seconds

311  
 312 **5.2. Release terminated, propagation continues**

313  
 314 Let the front of the plume has reached the position of the disc  $I$  just at the moment when the release  
 315 has terminated. Propagation continues to the disc positions  $I+1, I+2, \dots, I+j$ . Fluence rate for the new  
 316 front cloud position at disc  $I+j+1$  is calculated from the previous position  $I+j$  according to the  
 317 recurrent formula:

$$\Phi(E_\gamma, R, i=j+1, \dots, I+j+1) = \Phi(E_\gamma, R, i=j, \dots, I+j) + \Phi(E_\gamma, R, I+j+1) - \Phi(E_\gamma, R, j+1) \quad (6)$$

319

320 Hence, the contribution from the leftmost disc of a parcel is skipped and the fluence  $\Phi(E_\gamma, R, I+j+1)$   
 321 induced by the new rightmost disc  $I+j+1$  is calculated according to 2-D integration (3). Similar  
 322 considerations lead to the recurrent expression for the total fluence  $\Psi$ :

$$\Psi(E_\gamma, R, i=1, \dots, I+j+1) = \Psi(E_\gamma, R, i=1, \dots, I+j) + \sum_{i=j+1}^{i=I+j+1} \Delta t_i \cdot \Phi(E_\gamma, R, i) \quad (7)$$

324

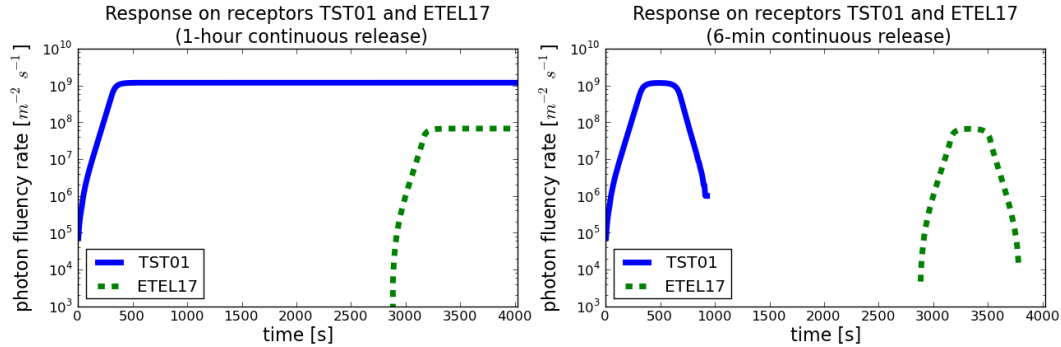
325 *Note: As mentioned in Chapter 2, the subsequent phases  $f>1$  are simulated using the SGPM*  
 326 *algorithm which performs a large number of elemental shifts driven by the new weather conditions.*  
 327 *Following Figure 1, the plume segment shift  $(s=1;f=1) \rightarrow (s=1;f=2)$  also proceeds generally in the*  
 328 *lateral direction. The concept of recurrent expressions cannot be applied here. We can use the*  
 329 *dispersion solution just after the shifts  $f \rightarrow f+1$ . The immediate values of the fluence rates related to*  
 330 *the new position of the plume in the end of the phase  $f+1$  can be easily calculated using the proposed*  
 331 *stepwise 2-D computational scheme. Nevertheless, for the later phases the formula for semi-infinite*  
 332 *cloud is usually accepted (depending on vertical homogenisation of the concentration). The direct*  
 333 *utilisation of the 3-D integration can be taken into consideration for some individual areas having a*  
 334 *special significance.*

335  
 336 **5.3. An illustrative example of application of the recurrent formulae**

337  
 338 We assume the release of radionuclide  $^{131}\text{I}$  with  $E_\gamma = 0,3625$  MeV ( $\gamma$ -yield is taken to be 100%, linear  
 339 attenuation coefficient  $\mu = 1.41\text{E-}02$  ( $\text{m}^{-1}$ ), linear energy absorption coefficient  $\mu_a = 3.30969\text{E-}03$  ( $\text{m}^{-1}$ )  
 340 (interpolated value). Mean free path values are  $1/\mu = 7.12\text{E+}01$  m,  $5/\mu = 3.56\text{E+}02$  m, and  $10/\mu =$



341 7.12 E+02 m. Time evolution of the fluencies/ fluence rates from one hour continuous activity release  
 342 9.0 E+14 Bq/hour of  $^{131}\text{I}$  (selected from Table 4) is simulated. Effective height  $h_{ef}$  of the release is 45  
 343 m, Pasquill categories of atmospheric stability F are examined (wind velocity at 10 m height  $u_{10}=1.0$   
 344  $\text{m}\cdot\text{s}^{-1}$ ). Short term meteorological forecast is for 20080111\_18 (January 11<sup>th</sup>, 2008, 18.00 CET), and  
 345 the wind blows in the direction of 273 deg.



346 **Figure 4.** Time evolution of responses on sensors TST01 and ETEL17 from the beginning of release with  
 347 continuous source strength 9.0 E+14 Bq/hour of  $^{131}\text{I}$ . Left: Continuous one-hour spreading . Right: Spread of  
 348 the shorter plume of 6 min. duration  
 349  
 350

351 Time evolution of the fluencies/ fluence rates for category F for sensors TST 01 and ETEL17 (roughly  
 352 400 m and 4 000 m respectively in direction of the plume propagation) is simulated in Figure 4. Long  
 353 continuous release of  $^{131}\text{I}$  having duration 1 hour is examined by equations (4) and (5) (see left part).  
 354 The right side of Figure 4 concerns the spreading of shorter plume of 6 minutes duration. Within the 6  
 355 minute interval the propagation is treated by equations (4) and (5). After that the continuous release  
 356 stops and the cloud is torn away the source. The fluence rates and fluencies are then governed by  
 357 equations (6) and (7).  
 358

## 359 6. Tests and comparisons of results

360  
 361 The proposed algorithm is tested for various release dynamics and model parameters. The method  $m/\mu$   
 362 was examined for  $m=5$  and  $m=10$  but the differences are small (a few per cent). The calculations for  
 363  $m=5$  are more than three times faster in comparison with  $m=10$ . Verification of the numerical  
 364 integration algorithm expressed in equations (3) is accomplished in Appendix A. The numerical results  
 365 are compared with the analytical solution of equation (3) for a special case without absorption ( $\mu=0$ )  
 366 and build-up factor  $B=1$  (a simplified experiment - “irradiation in vacuum”). Convergence to the semi-  
 367 infinite cloud solution is examined in Section 6.3.  
 368

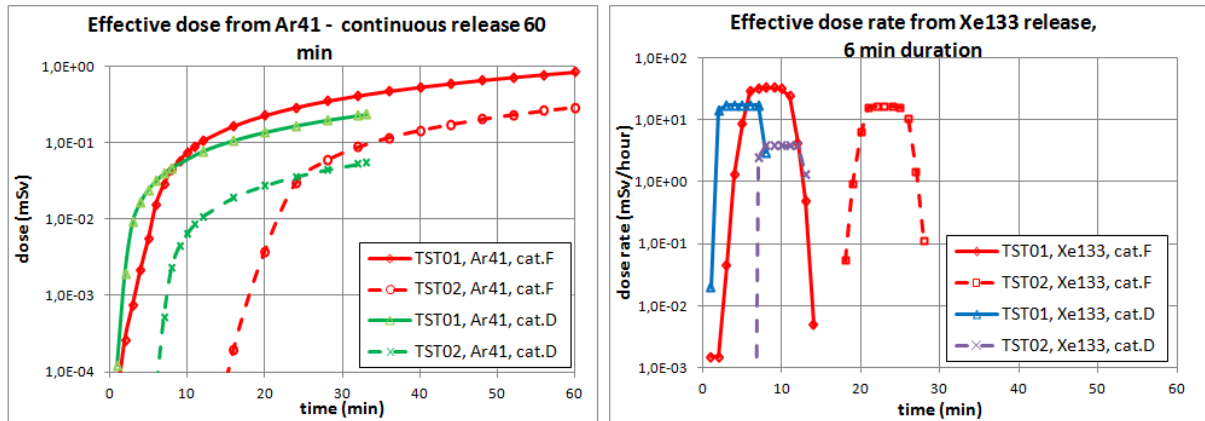
### 369 6.1. Derivation of the external irradiation dose from the photon fluencies

370  
 371 At first we shall formulate the relationship between the photon fluency/fluence rate and the individual  
 372 effective dose/dose rate of external irradiation from the cloud. The irradiation dose rate at the receptor  
 373 R is denoted by  $H(E_\gamma, R, i=1, \dots, I)$  ( $\text{Gy}\cdot\text{s}^{-1}$ ). It represents the irradiation from monoenergetic photons  
 374 with energy  $E_\gamma$  emitted from the whole plume (with the disc I in the front). It can be calculated from  
 375 the fluence rates (see equations (4) or (6) ) according to:  
 376

$$377 \quad H(E_\gamma, R, i=1, \dots, I) = \frac{\omega \cdot K \cdot \mu_a \cdot E_\gamma}{\rho} \cdot \Phi(E_\gamma, R, i=1, \dots, I) \quad (8)$$

378 Conversion factor  $K = 1.6 \text{ E}10^{-13} \text{ Gy}\cdot\text{kg}\cdot\text{MeV}^{-1}$ ;  $\omega = 1.11$  is a ratio of the absorbed dose in tissue to  
 379 the absorbed dose in air (more precise energy dependence is mentioned in Table 3), and the air density  
 380  $\rho = 1.293 \text{ kg}\cdot\text{m}^{-3}$ . The other quantities for the release of radionuclide  $^{131}\text{I}$  were described in the  
 381 beginning of Section 5.3. Equation (8) stands for absorbed doses expressed in grays. Common practice  
 382 in the radiation protection field is to multiply the absorbed doses by relative biological effectiveness

383 factor  $F_q$  which accounts for different biological damage with regards to different types of ionizing  
 384 radiation. The corresponding radiological quantity is expressed in Sv (sieverts), where  $F_q = 1$  for  
 385 photons. Therefore, we shall express doses in the following text and graphs in units of Sv.  
 386

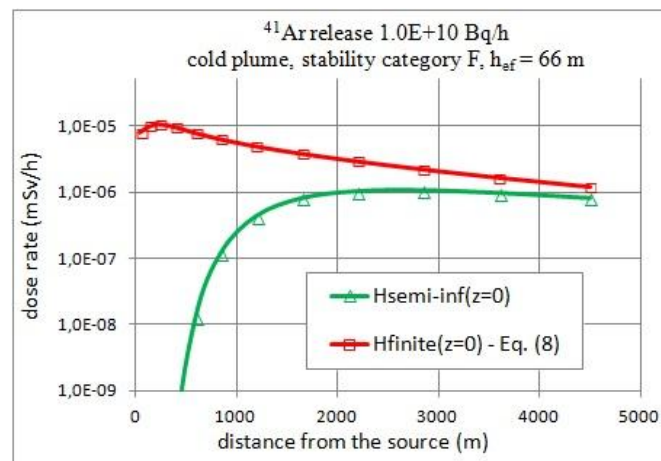


387  
 388 **Figure 5.** Time evolution of the effective individual cloudshine doses at positions of sensors TST01 and TST02  
 389 (400 m and 4 000 m respectively in the direction of the plume propagation). Continuous 1-hour release of  $^{41}\text{Ar}$   
 390 with strength  $3.33\text{E}+11 \text{ Bq}\cdot\text{s}^{-1}$  (left). Short 6-minute continuous release of  $^{133}\text{Xe}$  with strength  $2.78\text{E}+14 \text{ Bq}\cdot\text{s}^{-1}$   
 391 (right).  
 392

393 The application stemming from of equation (8) is given in Figure 5. The influence of the changing  
 394 meteorological conditions for Pasquill stability categories F and D ( $u_{10}=1.0 \text{ m}\cdot\text{s}^{-1}$  and  $3.0 \text{ m}\cdot\text{s}^{-1}$   
 395 respectively) is examined for two nuclides with different gamma energy levels.  $^{41}\text{Ar}$  has high photon  
 396 energy and long mean free path, while  $^{133}\text{Xe}$  has low photon energy and shorter mean free path (see  
 397 Table 3). The source strengths of both nuclides correspond to the values in Table 4. The dispersion  
 398 formulae KFK-Jülich for rough terrain are used.  
 399

### 400 6.2. Confrontation of the cloudshine doses generated nearby the source

401  
 402 Computer simulations are critical especially in high-consequence systems that can hardly ever be  
 403 tested in a fully representative environment. Plausibility of simulations can be tested also on consensus  
 404 of the computational simulations with the physical nature of the problem. An example of such partial  
 405 test is in Figure 6. Expected progress of both curves is confirmed. The proposed algorithm covers  
 406 realistically the ring of teledosimetric sensors located about 500 meters around the source.



407  
 408 **Figure 6.** Comparison of the finite cloud dose rates  $H_{\text{finite}}(z=0)$  calculated according to the proposed model  
 409 using equation (8) with the semi-infinite approach  $H_{\text{semi-inf}}(z=0)$ .  $E_\gamma = 1.2936 \text{ MeV}$  for radionuclide  $^{41}\text{Ar}$  ( $\gamma$ -yield  
 410 is 99.1%).  
 411

412 In the following text we shall carry out the convention comparison benchmark based on confrontation  
 413 of the results with several well-established international environmental codes. In the article (Bedwell  
 414 *et al.*, 2010) a hypothetical scenario of  $^{85}\text{Kr}$  discharge with intensity  $1.0 \times 10^{10} \text{ Bq.s}^{-1}$  over a 24 hour  
 415 period is analysed. Other characteristics were used: release height of 10 m, constant wind direction  
 416 with a speed of  $5 \text{ m s}^{-1}$ , a boundary layer depth of 800 m, heat flux of  $0 \text{ W m}^{-2}$ , representative Pasquill  
 417 stability category D, no rain, and terrain roughness of 0.3 m. Three receptor points are considered at 1,  
 418 2, and 5 km along the plume centre line. The effective cloud gamma dose rates are to be estimated,  
 419 averaged over 24 hours after the start of release. Monoenergetic photons having energy of 0.5300  
 420 MeV with yield  $4.340 \cdot 10^{-3}$  per decay are assumed according to (RadDecay, 1996). We have taken  
 421 Table 1 from (Bedwell *et al.*, 2010) related to the three significant European computer codes NAME  
 422 III (Lagrangian particle-puff trajectory model), ADMS 4 (3-D integration for calculation of photon  
 423 fluence, dispersion described by the new generation of Gaussian plume model based on advanced  
 424 parameterisation of the boundary layer structure) and PC CREAM (Gaussian quadrature for 3-D  
 425 numerical integration, dispersion using standard Gaussian plume model based on classical single  
 426 parameter Pasquill-Gifford stability categories). The original comparison from (Bedwell *et al.*, 2010)  
 427 was extended by our results (see Table 2). The outputs were generated by the environmental code  
 428 HARP (HARP, 2011) to which the new proposed algorithm for cloudshine doses estimation is fully  
 429 integrated.

430

431 **Table 2.** Model comparison for effective cloudshine dose rates for adults ( $\text{mSv.s}^{-1}$ ) at 3 sensors along the plume  
 432 centre line.

	NAME III <sup>a</sup>	ADMS <sup>a</sup>	PC CREAM <sup>a</sup>	HARP		
				Hosker (av. 24 hours)	Hosker (no averaging)	KFK
<i>1 km downwind</i>	$2.3 \cdot 10^{-09}$	$2.1 \cdot 10^{-09}$	$3.2 \cdot 10^{-09}$	$2.52 \cdot 10^{-09}$	$8.51 \cdot 10^{-09}$	$3.44 \cdot 10^{-09}$
<i>2 km downwind</i>	$1.1 \cdot 10^{-09}$	$8.2 \cdot 10^{-10}$	$1.3 \cdot 10^{-09}$	$1.04 \cdot 10^{-09}$	$4.07 \cdot 10^{-09}$	$1.47 \cdot 10^{-09}$
<i>5 km downwind</i>	$5.1 \cdot 10^{-10}$	$2.2 \cdot 10^{-10}$	$3.5 \cdot 10^{-10}$	$3.17 \cdot 10^{-10}$	$1.35 \cdot 10^{-09}$	$3.79 \cdot 10^{-10}$

433 <sup>a</sup> the values selected from (Bedwell *et al.*, 2010)

434

435 The HARP system is designed for sensitivity analysis and assessment of the "worst case" accidental  
 436 scenarios. User-friendly environment enables quick examination of variability for the input model  
 437 parameters. Three alternative formulae for horizontal dispersion  $\sigma_y$  are used to obtain the results  
 438 shown in Table 2. Hosker dispersion formulae are derived for smooth terrain using a sampling time of  
 439 10 minutes. Rough averaging of  $\sigma_y$  over a period of 24 hours was done using the recommendations  
 440 given in (Hanna, 1982) in order to fulfil the comparison requirements given above. For illustration,  
 441 results for  $\sigma_y$  related to the original sampling time of 10 minutes are also given in Table 2. The values  
 442 have evident physical meaning as instantaneous (un-averaged) dose rates. The results for KFK-Jülich  
 443 dispersion model presented in the last column in Table 2 can illustrate the sensitivity of the results  
 444 using the option of the alternative dispersion formulae for smooth versus rough terrain (KFK formulae  
 445 are predetermined for rough terrain of the Central European type). The results in Table 2 generated by  
 446 the HARP system in near distances from the source of pollution are well comparable with the  
 447 established international codes.

448

### 449 6.3. Verifying the convergence of the external $\gamma$ -exposure to the semi-infinite cloud solution

450

451 The dose conversion factor (DCF) for external exposure of a person submerged in the semi-infinite  
 452 cloud with uniform specific radioactivity of  $1 \text{ Bq.m}^{-3}$  represents a dose rate in units ( $\text{Sv.s}^{-1} \cdot \text{Bq}^{-1} \cdot \text{m}^3$ ).  
 453 The recommended factors are selected from (ICRP 74, 1996). The proposed algorithm was adjusted  
 454 for these special calculations. The value of radioactivity concentration  $C$  in equation (3) in ambient air

455 was assumed to be  $1 \text{ Bq}\cdot\text{m}^{-3}$  everywhere in any disc from the plume segmentation according to Figure  
 456 2. Three radionuclides with markedly different average photon energies were considered according to  
 457 Table 3. Segment thickness  $\Delta x$  is 10 m (see. equation (3)), Berger's formula for build-up factor is used  
 458 and the integration limit is  $5/\mu$  (see Figure 2). Here  $\omega$  is the ratio of effective dose to air dose for the  
 459 respective energy for isotropic irradiation geometry (ICRP 74,1996).

460 We can hardly expect an excellent agreement of our computations with a detailed DCF determination  
 461 based on Monte Carlo calculations with a human phantom model. Photon transport mechanisms are  
 462 simplified using empirical formulae (build-up factors, ratio  $\omega$ ). However, Table 3 shows good  
 463 agreement of the proposed algorithm with ICRP recommendations. At the same time, the results are  
 464 well comparable with findings of other authors, e.g. (Wang *et al.*, 2004) where 3-D integration is  
 465 substituted by a three-dimensional columned space subdivision on many finite grid cells, or (Armand  
 466 *et al.*, 2005) where a gamma exposure rate is simulated with 3-D Lagrangian particle model SPRAY  
 467 with the post-processor tool CLOUD\_SHINE.

468  
469

**Table 3.** Comparison of calculated dose rates with tabulated DCFs.

Nuclide	$\bar{E}^n$ (MeV)	$\omega(\bar{E}^n)$	$5/\mu$ (m)	Dose rate ( $\text{Sv}\cdot\text{s}^{-1}/(\text{Bq}/\text{m}^3)$ )	DCF (ICRP 74,1996) ( $\text{Sv}\cdot\text{s}^{-1}/(\text{Bq}/\text{m}^3)$ )
$^{41}\text{Ar}$	1.293	0.735	6.84E+02	5.47E-14 5.93E-14 <sup>a</sup>	6.50E-14
$^{131}\text{I}$	3.625E-01	0.666	3.56E+02	1.18E-14 1.545E-14 <sup>a,b</sup>	1.78E-14
$^{133}\text{Xe}$	5.230E-02	0.541	2.01E+02	1.62E-15	1.56E-15

470 <sup>a</sup> Higher integration limit up to  $10/\mu$ ; <sup>b</sup> Linear formula for build-up factor

471

472 The results shown in Table 3 are assumed to provide sophisticated particular evidence of proper  
 473 functionality of the proposed technique.

474

## 475 7. Accounting for multiple nuclide group

476

477 We assume the multiple photons  $p$  emitted with different energies  $E_p^n$  from radionuclide  $n$  which have  
 478 noticeable yields  $f_p^n$  (e.g. greater than 0.001). Following equation (8) the general expression for dose  
 479 rate ( $\text{Sv}\cdot\text{s}^{-1}$ ) from the multiple nuclides/multiple photons case can be rewritten as:

$$480 \quad H(R, i=1, \dots, I) = \sum_{(n)} H^n(R, i=1, \dots, I) = \frac{\omega \cdot K}{\rho} \sum_{(n)} \sum_{(p)} \mu_a(E_p^n) \cdot f_p^n \cdot E_p^n \cdot \Phi(E_p^n, R, i=1, \dots, I) \quad (9)$$

481 The corresponding dose in Sv can be calculated when substituting the fluence rate  $\Phi$  by the entire  
 482 photon fluence  $\Psi$  expressed by equation (5) or (7).

483

### 484 7.1. Averaging photon energies for each nuclide

485

486 Reduction of the computational load can be achieved by averaging the photon energies for the  
 487 nuclide  $n$  according to:

$$488 \quad \bar{E}^n = \sum_{(p)} f_p^n \cdot E_p^n / F^n; \quad F^n = \sum_{(p)} f_p^n \quad (10)$$

489 The subsequent simplified formulation for the dose rate is:

$$490 \quad H(R, i=1, \dots, I) = \sum_{(n)} H^n(R, i=1, \dots, I) = \frac{\omega \cdot K}{\rho} \sum_{(n)} \mu_a(\bar{E}^n) \cdot \bar{E}^n \cdot F^n \cdot \Phi(\bar{E}^n, R, i=1, \dots, I) \quad (11)$$

491 We have examined a hypothetical release of nuclide mixture illustrated in Table 4. Dependency of  
 492 physical coefficients on photon energy (for linear and mass attenuation coefficients, constants in build-  
 493 up factor formulae, etc.) is interpolated from discrete values prepared in (Pechova, 2012).

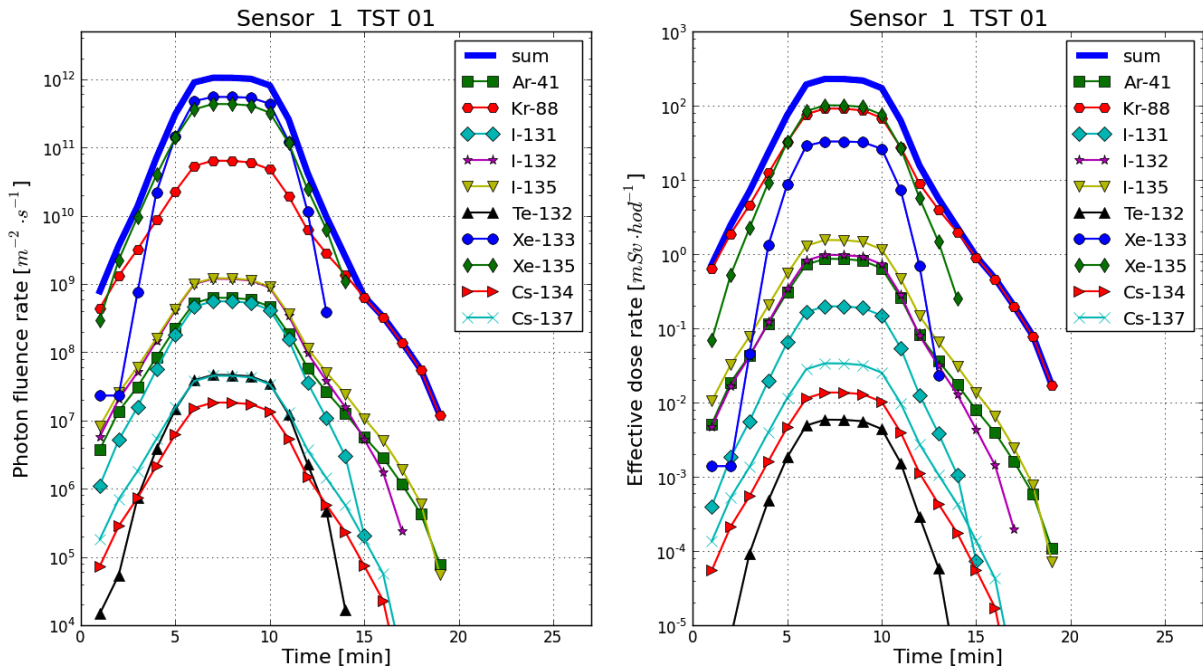
494  
495

**Table 4.** Hypothetical source term and averaged photon energies according to equation (10).

radionuclide	<sup>41</sup> Ar	<sup>88</sup> Kr	<sup>131</sup> I	<sup>132</sup> I	<sup>135</sup> I	<sup>132</sup> Te	<sup>133</sup> Xe	<sup>135</sup> Xe	<sup>134</sup> Cs	<sup>137</sup> Cs
activity release (Bq/hour)	1.2E+	1.2E+	9.0E+	2.2E+	2.2E+	5.5E+	8.2E+	6.6E+	3.2E+	7.9E+
$\bar{E}^n$ - eq. (10) in MeV	1.293	1.348	0.362	0.762	1.192	0.136	0.052	0.250	0.695	0.614
half-time of decay	1.8 h	2.8 h	8.01 d	2.3 h	6.6 h	78.6 h	5.2 d	9.1 h	2.06 y	30.0 y

496  
497  
498  
499

The outputs presented here are results of the model simulations using the proposed technique just at the points of existing fixed monitoring networks. The bilinear interpolation technique is used for determination of the values in an arbitrary location.



500  
501  
502  
503  
504

**Figure 7.** Response of sensor TST01 in the photon fluence rate (left) and dose rate (right) on a short release of 6-minutes duration. Sensor TST01 is located at a distance of about 400 m from the source, roughly in the direction of the plume propagation. Multi-nuclide source term is defined according to Table 4.

505  
506  
507  
508  
509  
510  
511  
512

Part of the results generated according to the simplified scheme (11) for sensor TST 01 is demonstrated for each nuclide in Figure 7. The radionuclide mixture is discharged into the atmosphere with a category stability class F. The effective height of release is  $h^{ef}=45$  meters, and wind speed at a height of 10 m is  $u_{10} = 1.0 \text{ m.s}^{-1}$ . Due to dependency of  $H$  in equation (11) on energy, the shape of curves for photon fluence rates (left) somewhat differs from the corresponding dose rates (right). The calculations for all nuclides and for all sensors are running in one stroke. A significant outcome is achieved by computation effectiveness, when the complete run for all nuclides and all sensors lasts about 90 seconds on a PC with a standard, common configuration.

513  
514  
515

### 7.2. Substitution of multi-nuclide approach to multi-group scheme

516  
517  
518  
519  
520  
521

Equation (3) is formulated for simplified case of a nuclide emitting one photon with average energy  $E_\gamma$  per decay. Some nuclides have a rather wide spectrum of emitted photons. We can expect a certain inaccuracy to be introduced to the results when using computational schemes (10) and (11) with only average energy. The straightforward solution offers a detailed scheme given by equation (9). But it could cause a huge escalation of computational load and the main goal of a real time analysis may not be achievable.

522 An alternative method is proposed here with the goal of making further calculations more accurate and  
523 at the same time sufficiently fast for a large group of nuclides discharged into the atmosphere. The  
524 whole range of possible photon energy levels is partitioned into  $G$  energetic groups:  $G=24$  and  
525 alternatively  $G=8$  were selected according to (Pechova, 2012; RadDecay, 1996). Probability and  
526 emitted energy values were extracted for each photon  $p$  of a cascade belonging to each nuclide from  
527 the nuclide mixture. Linear total gamma attenuation coefficients  $\mu$  and linear gamma energy-  
528 absorption coefficients  $\mu_a$  are interpolated on the basis of the same energetic separation. Let  ${}^n E_p^g$  stands  
529 for energy of each photon  $p$  emitted by the nuclide  $n$  having energy belonging to the group  $g$  with the  
530 yield of  ${}^n f_p^g$ . The mean energy  $\bar{E}^g(x_I)$  averaged over all photons emitted to the energy interval  $g$   
531 from all radionuclides  $n$  at downwind distance  $x_I$  can be found using the "source depletion" approach  
532 introduced in equation (1):  $A^n(x_I, y=0, z= h_{ef}) = A^n(x=0, y=0, z= h_{ef}) \cdot f_R^n(x_I) \cdot f_F^n(x_I) \cdot f_W^n(x_I)$ . The  
533 values of  $\bar{E}^g(x_I)$  are determined according to equation (12). Depletion factors for dry and wet  
534 deposition  $f_F^n(x_I)$  and  $f_W^n(x_I)$  have to be distinguished according to the physical-chemical forms of  
535 radionuclides, land use characteristics of the terrain and precipitation intensity - more details can be  
536 found in the documentation of the HARP product (HARP, 2011).

$$537$$

$$538 \quad \bar{E}^g(x_I) = \frac{\sum_{n=1}^N A^n(x_I) \cdot \bar{E}_n^g \cdot F_n^g}{\sum_{n=1}^N A^n(x_I) F_n^g}; \quad \bar{E}_n^g = \sum_{(p(n))} {}^n E_p^g \cdot {}^n f_p^g; \quad F_n^g = \sum_{(p(n))} {}^n f_p^g \quad (12)$$

539  
540 The denominator in equation (12) represents the total number of photons emitted in disc  $I$  per second  
541 from all nuclides belonging to the group  $g$ . Now we introduce an expression for the photon fluence  
542 rate from the total number of photons emitted from all nuclides belonging to the energetic group  $g$ .  
543 After separation of the nuclide part and the spatial integration part, equation (3) can be rewritten as:

$$544 \quad \Phi^g(\bar{E}^g(x_I), R, I) = SUM(x_I; g) \cdot INTEG(x_I; R, g) \quad (13)$$

$$545$$

$$SUM(x_I; g) = \sum_{(n)} A^n \cdot f_R^n(x_I) \cdot f_F^n(x_I) \cdot f_W^n(x_I) \cdot \bar{E}_n^g$$

$$548 \quad INTEG(x_I; R, g) = \frac{\Delta x}{4\pi} \int_{r=0}^{r_{\max}} \int_{\phi=0}^{2\pi} \frac{DISPER(x_I; y, z) \cdot B(\bar{E}^g(x_I), \mu(\bar{E}^g(x_I)) \cdot d) \cdot \exp(-\mu(\bar{E}^g(x_I)) \cdot d)}{d^2} r d\phi dr$$

$$549 \quad DISPER(x_I; y = y(r, \phi), z = z(r, \phi)) = \frac{1}{2\pi \cdot \sigma_y(x_I) \cdot \sigma_z(x_I) \cdot \bar{u}} \exp\left(-\frac{y^2}{2\sigma_y^2(x_I)}\right) \left[ \exp\left(-\frac{(z - h_{ef})^2}{2\sigma_z^2(x_I)}\right) + \right.$$

$$550 \quad \left. + \exp\left(-\frac{(z + h_{ef})^2}{2\sigma_z^2(x_I)}\right) + \exp\left(-\frac{(z - 2H_{mix} + h_{ef})^2}{2\sigma_z^2(x_I)}\right) + \eta_{JV}(z) \right]$$

551  
552 Where INTEG is expressed in analogy with equation (1), but specifically stands for distribution of the  
553 fluence rate of photons at receptor point  $R$  from all nuclides contributing to the energetic group  $g$ . The  
554 resulting values are given by summing over all energetic groups  $g$ . It substitutes the former procedure  
555 based on the cycle over all nuclides.

### 557 7.3. Performance of multi-group approximation

558  
559 The main achievement of the outlined technique illustrated above is the fact, that the time consuming  
560 integration INTEG is nuclide independent. Earlier repetitive estimation for each nuclide (or in detail  
561 for each photon  $p$  emitted by a nuclide described by equation (9)) can be avoided. This alternative  
562 scheme is assumed to accelerate calculations for the scenarios with a large number (several tens) of  
563 discharged nuclides. For a medium group of 10 nuclides from Table 4, the former calculations  
564 according to expression (11) (run1) are compared with the multi-group approach for a fine resolution

565 into 24 energetic groups (run2) and a rough resolution into 8 groups (run3). The computation of run3  
566 is about three times faster than run2 and about 2.5 times faster than run1. The substantial advantage  
567 will be brought for large nuclide groups. The computational time of run1 is expected to be linearly  
568 proportional to the nuclide count while the computational time of the multi-group approach will be  
569 more or less constant, regardless of the increasing count of nuclides. As for dose estimates, for the  
570 medium nuclide group from Table 4, a small mutual differences have occurred. More systematic  
571 examination should be carried out for scenarios with a large number of released nuclides. Grouping of  
572 the gamma rays according to energies was extended (Pechova, 2012) for additional nuclides belonging  
573 to an extensive release of a hypothetical radiation accident. A hypothetical severe accident with the  
574 training source term ST2 selected from the RODOS system has been now recalculated using the  
575 proposed multigroup scheme. The scenario is initiated by LOCA accident (Loss of Cooling Accident)  
576 in combination with the subsequent events described in (Pechova, 2003). A large group of discharged  
577 radionuclides is taken into account (37 in total). The conclusion related to the performance of the  
578 multigroup scheme was verified.

579

## 580 **8. Discussion and conclusions**

581

582 A fast algorithm is presented for estimation of external irradiation from radioactive cloud nearby the  
583 source of pollution. The proposed unconventional finite cloud approach avoids the severe  
584 underestimation of cloudshine doses nearby the source arising from utilisation of the formerly used  
585 semi-infinite plume model. Thanks to its fast and effective operation this solution supports potency of  
586 the advanced consequence assessment techniques for improvement of emergency preparedness and  
587 management. The proposed method provides simulation of time and space evolution of cloudshine  
588 doses in the early phase of an accident in a real-time mode and on a detailed timescale. Large mixtures  
589 of discharged nuclides can be effectively treated simultaneously when the usual multi-nuclide  
590 approach is substituted by the new multi-group scheme. This software tool is incorporated into the  
591 routine operation of the environmental code HARP (HARP, 2011) with the aim for it to serve as a  
592 proper component supporting the advanced data assimilation techniques to be computationally feasible  
593 (Pecha *et al.*, 2009; ASIM, 2012; Hofman *et al.*, 2013). An experience with the particle filter  
594 sampling approximation was gained there for the solution of this complex task, which is analytically  
595 intractable.

596 Large uncertainties involved in an accident scenario and information noise occurring in the beginning  
597 of a calamity constitute a cardinal problem for the decision making staff. For example the uncertainty  
598 in the source term dominates among all other uncertainties of an accidental release scenario.  
599 Estimated radiological values can differ from the true ones by a factor of 10 or more. An improvement  
600 of the dose predictions in the specific nearest vicinity of the source of pollution taking into account the  
601 teledosimetric ring of sensors on fence of the nuclear power facility plays a decisive role in the source  
602 term re-estimation and inverse modelling. Such extraction of information from observations for the  
603 model parameter improvement increases credibility of the consequence assessment. The predictions of  
604 the potentially affected areas and the corresponding contamination levels can be recursively  
605 reconstructed.

606 Practically all advanced assimilation methods perform computationally expensive multiple repetitive  
607 recall of the environmental model. Hence the formulation of a fast and effective routine for  
608 determination of the external irradiation doses is of a crucial significance. It has to comply with other  
609 specific requirements in order to cover a large net of measuring apparatus located on the terrain which  
610 should include both fixed stations and various sensors on potential mobile vehicles. Furthermore, the  
611 routine is capable of managing the problem of a large mixture of discharging radionuclides when a  
612 new multi-group approach is introduced.

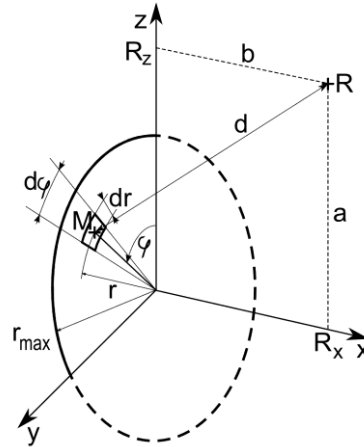
613 This article addresses here only the cloudshine dose calculations. However, the measuring devices  
614 detect cloudshine and groundshine doses in total. For assimilation purposes a simplified assessment of  
615 contribution from the activity deposited on the ground (based on tabulated conversion factors) to the  
616 external irradiation has been applied (Pecha *et al.*, 2009, Smidl *et al.*, 2013). In this conservative case  
617 an individual is assumed to be standing on a smooth infinite plane with a uniform source  
618 concentration. More detailed examinations should be related to additive modifying factors taking into

619 account the effects of ground roughness and non-uniform source distribution. For these particular  
 620 cases an effect of a possible near-standing shielding object should be taken into consideration.  
 621 Finally, it should be pointed out that the originated plume segmentation method based on the stepwise  
 622 2-D computational approach presented here can be considered a certain fast dispersion scheme  
 623 alternative to the puff model.  
 624

## 625 **Appendix A. Verification of the proposed algorithm for numerical integration**

626  
 627 The photon fluence rate given by expression (3) is integrated numerically using the Gauss-Legendre  
 628 integration formula which is the most commonly used form of Gaussian quadratures. The Gaussian  
 629 quadratures provide the flexibility of choosing not only the weighting coefficients but also the  
 630 locations (abscissas) where the function values are evaluated. The Gauss-Legendre formula is based  
 631 on the Legendre polynomials of the first kind  $P_m(x)$ . For the chosen degree  $m$  of the polynomial we  
 632 have tested the limits of its applicability on a given experimental configuration illustrated in Figure 8.  
 633 An emitting disc with optional the radius  $r_{max}$  is located in the plane  $(y,z)$  with its centre in the origin of  
 634 the coordinate system. We assume that without restriction to generality we can simplify the  
 635 expression (3) in three manners:

- 636 ○ Uniform radioactivity concentration on the disc surface is assumed ( $C(x; r, \varphi) = 1 \text{ Bq/m}^2$ )
- 637 ○ No photon absorption takes place in the medium between the disc and the receptor point R  
 638 ( $\mu=0$ )
- 639 ○ The photons are emitted from the disc elements isotropically and without any secondary  
 640 collision on their path from the source up to the receptor point (the build-up factor is 1)



641  
 642 **Figure 8.** Disc in plane  $(y,z)$  irradiating the receptor R.  
 643

644 With exaggeration, it can be perceived as a “vacuum experiment” for the disc and receptors located  
 645 in the outer space. Photon fluence rate ( $m^{-2} s^{-1}$ ) is now expressed by simplified equation (3):

$$646 \quad \Phi(E_\gamma, R) = \frac{1}{4\pi} \int_{r=0}^{r_{max}} \int_{\varphi=0}^{2\pi} \frac{1}{d^2} r d\varphi dr \quad (14)$$

647 According to Figure 8 the distance  $d$  between the sensor R and elemental surface  $r d\varphi dr$  equals to

$$648 \quad d = d(r, \varphi) = \sqrt{a^2 + b^2 + r^2 - 2 \cdot r \cdot a \cdot \cos \varphi}$$

649 Equation (14) can be integrated analytically and the number of photons crossing  $1 \text{ m}^2$  per second at the  
 650 position of the sensor R is expressed as:

$$651 \quad \Phi(E_\gamma, R) = \frac{1}{4} \ln \left( \frac{r_{max}^2 + b^2 - a^2 + \text{sqr}t \left( r_{max}^4 + 2r_{max}^2 (b^2 - a^2) + (a^2 + b^2)^2 \right)}{2b^2} \right) \quad (15)$$



652 A 30-point Gauss-Legendre integration formula is used to numerically integrate equation (14) for  
 653 various ranges of constants  $a$  and  $b$ . A partial comparison of numerical and analytical values is  
 654 presented in Table A1. Additional tests revealed a certain numerical instability for a case when the  
 655 sensor  $R$  lies in the plane of the disc ( $b=0$ ) and constant  $a$  is approaching zero. In this instance we are  
 656 using the lowest value of constant  $b$  slightly above zero ( $b \cong 0.2$  m).  
 657

658 **Table A1.** Comparison of numerical and analytical values of photon fluence rate for various values  $a$ ,  $b$  of  
 659 sensor  $R$  positions. Radius of the radiating disc is  $r_{max}=49$  m.  
 660

a (m)	b (m)	Photon fluence rate $\Phi$ ( $m^{-2}s^{-1}$ )	
		analytically – see (15)	numerically – see (14)
144	144	1.446555 E-02	1.446555 E-02
60	60	8.189546 E-02	8.189548 E-02
10	10	7.950500 E-01	7.950501 E-01
1.0	1.0	1.945767 E+00	1.945910 E+00
0.5	0.5	2.290156 E+00	2.292484 E+00
0.2	0.2	2.744151 E+00	2.750629 E+00
0.1	0.1	3.064821 E+00	3.097203 E+00

661

## 662 Acknowledgements

663 These activities are supported thanks to Project No. VG20102013018, Ministry of the Interior of the  
 664 Czech Republic.

665

## 666 References

667

- 668 Abida R and Bocquet M 2009 Targeting of Observations for Accidental Atmospheric Release Monitoring *Atmospheric*  
 669 *Environment* **43** 40
- 670 ADMS 2009 Calculation of  $\gamma$ -Ray Dose Rate from Airborne and Deposited Activity *CERC Cambridge Environmental*  
 671 *Research Cons. Ltd Cambridge ADMS4 P/20/01L/09*
- 672 Armand P Achim P Monfort M Carrere J Oldrini O Commanay J and Albergel A 2005 Simulation of the plume gamma  
 673 exposure rate with 3D Lagrangian particle model SPRAY and post-processor CLOUD-SHINE *Proc. 10th Int.*  
 674 *Conf. on Harmonisation within Atm. Dispersion Modelling for Regulatory Purposes* (Crete, Greece) pp 545-550
- 675 ASIM 2012 ASIM - A software Tool for Assimilation of Model Predictions with Observations from Terrain. URL:  
 676 <http://asim.utia.cas.cz/>
- 677 Bedwell P Wellings J Haywood S M and Hort M C 2010 Cloud Gamma Modelling in the UK MET Office's NAME III  
 678 Model. *Proc 13th International Conference on Harmonisation within Atmospheric Dispersion Modelling for*  
 679 *Regulatory Purposes* (Paris, France) pp 441-444
- 680 Doucet A, De Freitas N and Gordon N 2001 Sequential Monte Carlo methods in practice *Springer Verlag*
- 681 HARP 2011 HARP - HAZardous Radioactivity Propagation: A Software Tool for Fast Assessment of Radiological  
 682 Consequences of Radiation Accident URL: <http://havarrp.utia.cas.cz/harp/>
- 683 Hanna S Briggs R G A and Hosker Jr R P 1982 Handbook on Atmospheric Diffusion *DOE/TIC-11223* (DE82002045)
- 684 Hofman R and Pecha P 2011 Application of Regional Environmental Code HARP in the Field of Off-site Consequence  
 685 Assessment *PSA 2011 International Topical Meeting on Probabilistic Safety Assessment and Analysis* American  
 686 Nuclear Society (Wilmington NC, USA)
- 687 ICRP 1996 Conversion Coefficients for use in Radiological Protection against External Radiation *ICRP Publication 74 Ann.*  
 688 *ICRP* **26** (3-4)
- 689 Overcamp T J 2007 Solutions to the Gaussian Cloud Approximation for Gamma Absorbed Dose *Health Physics* **92** 78 – 81
- 690 Päsler-Sauer J 2000 Description of the Atmospheric Dispersion Model ATSTEP *RODOS(WG2)-TN(97)-01 KFK, Karlsruhe*
- 691 Pecha P and Hofman R 2011 Construction of observational operator for cloudshine dose from radioactive cloud drifting over  
 692 the terrain *Proc. 14th International Conference on Harmonisation within Atmospheric Dispersion Modelling for*  
 693 *Regulatory Purposes* (Kos Island, Greece) pp 732-736
- 694 Pecha P Hofman R and Šmídl V 2009 Bayesian tracking of the toxic plume spreading in the early stage of radiation accident.  
 695 *Proc. of European Simul. and Modelling Conference ESM*
- 696 Pecha P and Pechova E 2002 Application of the COSYMA code for comparative analysis of a certain accidental releases of  
 697 radioactivity *Proc. 4th International conference IMUG2002 (Principality of Monaco), BNL Upton* pp 5-15
- 698 Pechova E 2012 Grouping of gamma rays according to energies *Research report of Nuclear Research Institute Dpt. EGP*  
 699 Prague EGP 5014-F-120987
- 700 Pechova E 2003 Calculation of radioactivity propagation - Joint Czech-Austrian Workshop, Vienna *Research report of*  
 701 *Nuclear Research Institute Dpt. EGP Prague EGP 5014-J-030152*

702 RadDecay 1996 Radioactive Nuclide Library and Decay Software - Version 1.13 for WINDOWS *Grove Engineering*  
703 Rockville, Maryland

704 Raza S S Avilla R and Cervantes J 2001 A 3-D Lagrangian (Monte Carlo) Method for Direct Plume Gamma Dose Rate  
705 Calculations *Journal of Nuclear Science and Technology* **38** (4) 254-260

706 Slade D M 1968 Meteorology and Atomic Energy *USAEC TID 24190-1968*, Russian translation

707 Šmídl V Hofman R and Pecha P 2013 Evaluation of detection abilities of monitoring networks using different assessment  
708 criteria *15th Int. Conf. on Harmonisation within Atmospheric Dispersion Modelling for Regulatory Purposes*  
709 (Madrid, Spain)

710 Smith J G and Simmonds J R (Eds.) 2008 The Methodology for Assessing the Radiological Consequences of Routine  
711 Releases of Radionuclides to the Environment Used in PC-CREAM 08 *Research Report HPA-RPD-058 Health*  
712 *Protection Agency* (Chilton, Didcot, UK)

713 Thykier-Nielsen S Deme S and Láng E 1995 Calculation Method for Gamma Dose Rates from Gaussian Puffs *RISO*  
714 *National Laboratory, Roskilde, Denmark, RISO-R-775(EN)*

715 Wang X Y Ling Y S and Shi Z Q 2004 A new finite cloud method for calculation external exposure dose in a nuclear  
716 emergency *Nuclear Engineering and Design* **231** 211-216

717